DEVELOPMENT AND USE OF NANOPARTICLES TO STUDY THE BIOLOGICAL MECHANISM OF CARBOHYDRATE LEWIS^{A} BINDING DURING BRAIN INFLAMMATION



A thesis submitted for the degree of Doctor of Philosophy

Department of Pharmacology

University of Oxford

Kim Wals

Somerville College ▪ University of Oxford

Trinity 2018

To my father, who was a great builder.

I wish you could have seen me build.

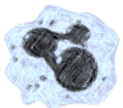
| ABBREVIATIONS |

^{13}C	Carbon, isotope 13
^{1}H	Proton, hydrogen isotope 1
A.U.	Arbitrary Units
AA	Acetic Acid
ABO	Antigen A, B and none for blood group
Ac	Acetyl, Acetate
AcN	Acetonitrile
AD	Alzheimer's disease
ALS	Amyotrophic lateral sclerosis
ALY	A-typical Lymphocyte
APC	Antigen Presenting Cell
APDMES	3-Aminopropyl-Dimethyl-Ethoxysilane
APR	Acute Phase Response
APTES	3-Aminopropyl-Trimethoxysilane
Au	Gold
AURE	AU-rich sequences
BASO	Basophil
BBB	Blood Brain Barrier
BCG	Bacille Calmette-Guèrin
BDNF	Brain-Derived Neurotrophic Factor
BG	Basal Ganglia
BIAB	Bis(acetoxy)iodobenzene
BSA	Bovine Serum Albumin
C	Celcius
C3…	Complement component 3 (and numbers thereof)
CAN	Ceric Ammonium Nitrate
CCL	Chemokine (C-C motif) Ligand
CD	Cluster of Differentiation
cDNA	Copy Deoxyribonucleic acid
CFA	Complete Freund's Adjuvant
CNS	Central Nervous System
COL1A1	Collagen 1 Alpha 1 (and numbers thereof)
conc.	Concentration
COSY	Correlation Spectroscopy
CSF	Cerebrospinal fluid
CT	Computed Tomography or Cycle Threshold
Ctr1	Copper Transport Protein 1
C-Type	Calcium-binding, for C-Type Lectins
CXCL	Chemokine (C-X-C motif) Ligand
d	Doublet
DAB	3,3'-Diaminobenzidine
DBU	1,8-Diazabicyclo[5.4.0]undec-7-ene
DCM	Dichloromethane
DCs	Dendritic cells
DC-SIGN	DC-Specific ICAM-3 Grabbing, Nonintegrin
dd	Doublet of doublet
DIPEA	Diisopropylethylamine
DLS	Dynamic Light Scattering
DMAP	4-Dimethylaminopyridine
DMF	*N,N*-dimethylformamide
DMSO	Dimethyl Sulfoxide
DNA	Deoxyribonucleic acid
DNP	Dynamic Nuclear Polarisation
dt	Doublet of triplets
DTBMP	2,6-Di-Tert-Butyl-4-Methylpyridine
DTBS	Di-Tertbutylsilylene
EAE	Experimental Autoimmune/Allergic Encephalomyelitis
EDC	N-(3-Dimethylaminopropyl)-N'-ethylcarbodiimide hydrochloride
EDTA	Ethylenediaminetetraacetic acid
EGFR	Epidermal Growth Factor Receptor
ELISA	Enzyme-Linked Immunosorbent Assay
EOS	Eosinophil
equiv.	Equivalents
E-Selectin	Endothelial-Selectin
EST	Expressed Sequence Tag
EtOAc	Ethyl acetate
EtOAc	Ethyl Acetate
eV	Electronvolt
FBS	Fetal Bovine Serum
EV	Extracellular Vesicle
Fe	Iron
Fmoc	9-Fluorenylmethoxycarbonyl
FT-IR	Fourier-Rransform Infrared spectroscopy
Fuc	Fucose
FUT	Fucosyl Transferase
g	Grams
Gal	Galactose
Gd	Gadolinium
GlcNAc	*N*-Acetyl Glucosamine
Gly	Glycine
GPCRs	G-Protein Coupled Receptors
h	Hour
HATU	(1-[Bis(dimethylamino) methylene]-1H-1,2,3-triazolo[4,5-b]pyridinium 3-oxid hexafluorophosphate

HCT	Hematocrit
HGB	Heamoglobin
HLA	Human Leukocyte Antigen
HSQC	Heteronuclear single quantum coupling
Hz	Hertz
ICAM	Intercellular Adhesion Molecule
ICE	Interleukin-1 Converting Enzyme
IgG	Immunoglobulin type G
IL	Interleukin
IL-1R	Interleukin-1 Receptor
IL-1RA	IL-1-receptor antagonist
IL-1β	Interleukin-1 Beta
IME	2-imido-2-methoxyethyl
J	Coupling constant
K	Kilo
L	Liter
LCN2	Lipocalin-2
Le	Lewis
Le$^{a\,(b,x,y)}$	Lewis a, b, x, y
LFA-1	Lymphocyte Function-Associated Antigen 1
LIC	Large Immature Cell
LNDFH	Lacto-*N*-difucohexose
LNFP	Lacto-*N*-fucopentaose
LNnDFH	lacto-*N*-*neo*difucohexaose
LPS	Lipopolysaccharide
L-Selectin	Lymphocyte-Selectin
LYMPH	Lymphocyte
M	Molar
m	Multiplet, milli
M N	M and L alleles for blood group
MASP	MBL Associated Serine Proteases
MBL	Mannan Binding Lectin
MBP	Myelin Basic Protein
MCH	Mean Corpuscular Haemoglobin
MCHC	Mean Corpuscular Haemoglobin Concentration
MCP-1	Monocyte Chemoattractant Protein 1
MCV	Mean Corpuscular Volume
Me	Methyl
MeOH	Methanol
MES	2-(N-Morpholino)ethanesulfonic acid
MHC	Major Histocompatibility Complex
miRNA	Micro Ribonucleic Acid
mMPIO	Multimeric Magnetic (nano)-Particles of Iron Oxide
MOG	Myelin Oligodendrocyte Glycoprotein
MONO	Monocyte
MPIO	Magnetic (nano)-Particles of Iron Oxide
MPV	Mean Platelet Volume
MRI	Magnetic Resonance Imaging
mRNA	Messenger Ribonucleic Acid
MS	Multiple Sclerosis
MS*	Mass Spectromtery
MS4Å	Molecular sieves 4 angstroms
mV	Milli Volt
MWCO	Molecular Weight Cut-Off
n	Nano
NADPH	Nicotinamide Adenine Dinucleotide Phosphate
NEUT	Neutrophil
NF-κB	Nuclear factor kappa B
NGAL	Neutrophil Gelatinase-Associated Lipocalin
NHS	N-Hydroxysuccinimide
NMDA	(*N*-methyl-D-aspartate)
NMR	Nuclear Magnetic Resonance
NP	Nanoparticles
NTA	Nanoparticle Tracking Analysis
OCB	Oligo Clonal Band
OCT	Optimal Cutting Temperature
ON	Overnight
OXT	Oxyotocin
P/S	Penicillin / Streptomycin
PBS	Phosphate Buffered Saline
PCR	Polymerase Chain Reaction
PCT	Plateletcrit
PD	Parkinson's disease
PE	Petroleum Ether
PECAM-1	Platelet Endothelial Cell Adhesion Molecule-1
PET	Positron Emission Tomography
Ph	Phenyl
PLP	Proteolipid Protein
PLT	Platelet
PMB	Para-methoxyphenyl (4-methoxyphenyl)
PMN	Polymorphonuclear
PS	Polystyrene
P-Selectin	Platelet-Selectin
PSGL-1	P-Selectin Glycoprotein Ligand-1
PTM	Post Translational Modification
PXL	Photo-crosslinker
q	Quartet
qPCR	Quantitative Polymerase Chain Reaction
quant.	Quantitative
RBC	Red Blood Cell
RDW	Red cell Distribution Width
Rh	Rhesus for blood group
RIPA	Radio-Immunoprecipitation Assay buffer

ROI	Region of Interest
ROS	Reactive Oxygen Species
RT	Room Temperature
s	Singlet
sat.	Saturated
SCM	S-cyanomethyl
Se	Secretor
Si	Silicon
SIGN-R3	C-type lectin receptors specific intracellular adhesion molecule-3 grabbing non-integrin homolog-related 3
sIL-1R1	soluble type I Interleukin-1 receptor
sIL-1R2	soluble type II Interleukin-1 receptor
sIL-1RAcP	soluble Interleukin-1-receptor accessory protein
siRNA	Small interfering Ribonucleic Acid
SLC…	Solute Carrier transport protein (and numbers thereof)
sLe^x	Sialyl-Lewis x
SOD	Super Oxide Dismutase
SCM	S-Cyanometyl
STDEV	Standard Deviation
t	Triplet
TBI	Traumatic Brain Injury
TBS	Tert-Butyldimethylsilyl (TBDMS)
TBSCl	Tert-Butylchlorodimethylsilane
TEMPO	(2,2,6,6-Tetramethylpiperidin-1-yl)oxyl
THF	Tetrahydrofuran
Ti	Titanium
TLC	Thin Layer Chromatography
TMS	Trimethylsilyl
TNF-α	Tumor Necrosis Factor Alpha
TsCl	Tosyl Chloride
TTR	Transthyretin
USPIO	Ultra-Small Particles of Iron Oxide
UV	Ultra-Violet
VCAM-1	Vascular Cell Adhesion Molecule 1
VLA-4	Very Late Antigen-4
W	Watt
WBC	White Blood Cell
XPS	X-ray Photoelectron Spectroscopy,
XRF	X-Ray Fluorescence
Zr	Zirconium
ζ	Zeta
µ	Micro

Image representations used throughout thesis (not to scale)


Neutrophil


Platelet

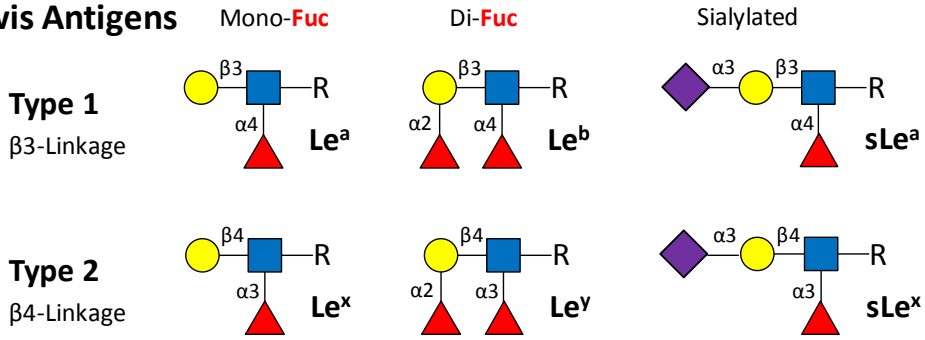

Nanoparticle (MPIO)


Endothelial Cell


E / L / P Selectin


Antibody

Lewis Antigens



Symbolic Representation of Monosaccharides Used

Galactose (**Gal**)

Fucose (**Fuc**)

N-Acetyl Glucosamine (**GlcNAc**)

Sialic acid (*N*-Acetyl Neuraminic acid (**Neu5Ac**))

R = lipid, protein, glycan, nanoparticle…

| TABLE OF CONTENT |

I…		**Dedicated to…**
II…		**| ACKNOWLEDGMENTS I**
IV…		**| ABBREVIATIONS |**
VII…		**| TABLE OF CONTENT |**
XIV…		**| LISTING OF FIGURES AND TABLES |**
1…	**1**	**|INTRODUCTION |**
		INTRODUCTION TO BRAIN INFLAMMATION BIOLOGY AND TARGETED IMAGING STRATEGIES USING NANOPARTICLES
3…		**INTRODUCTION OVERVIEW**
4…	**1.1**	**| INFLAMMATION, CELL ADHESION AND CARBOHYDRATES**
4…	**1.1.1**	The blood brain barrier
4…	**1.1.1.1**	The blood brain barrier and immune cell infiltration during inflammation
6…	**1.1.2**	IL-1β: A potent inflammatory cytokine
6…	**1.1.2.1**	IL-1β | Transcriptional regulation
7…	**1.1.2.2**	IL-1β | Protein production
7…	**1.1.2.2**	IL-1β | Protein regulation
8…	**1.1.3**	Cell adhesion molecules in inflammation
12…	**1.1.4**	Carbohydrate ligands for lectins and multivalent interactions
14…	**1.1.4.1**	Lewis antigens in brain inflammation
16…	**1.1.4.2**	The historic discovery of Lewis antigens
16…	**1.1.4.3**	Bio-distribution and synthesis of Lewis antigens
19…	**1.1.4.4**	E- and P-Selectin in the CNS
20…	**1.1.4.5**	Lewis antigens and binding to Selectins is assay dependent
22…	**1.1.4.6**	Other Lewis^{a}-binding lectins
22…	**1.1.4.6.1**	Mannan Binding Lectin (MBL)
23…	**1.1.4.6.2**	DC-SIGN (CD209)
25…	**1.2**	**| MULTIPLE SCLEROSIS**
25…	**1.2.1**	Introduction to MS
25…	**1.2.2**	Immune cell infiltration and the brain vasculature in MS
26…	**1.2.2.1**	MS | T Cells
26…	**1.2.2.2**	MS | B Cells
27…	**1.2.2.3**	MS | Microglia and macrophages
27…	**1.2.3**	Other aspects of MS –vessels and vesicles
30…	**1.2.4**	MS and MRI imaging of inflammation
33…	**1.2.5**	Proteomics and genomics of MS and animal models of MS
34…	**1.2.5.1**	MS | EAE and BCG animal models

35… **1.2.5.2** MS | Genomics and transcriptomics
36… **1.2.5.3** MS | Proteomics
38… **1.2.5.4** Proteomic identification of targets using photo-crosslinkers

42… **1.3** **| NANOPARTICLES FOR ALTERNATIVE IMAGING MODALITIES**
42… **1.3.1** Introduction to nanoparticles as imaging modalities
42… **1.3.2** X-Ray fluorescence imaging
43… **1.3.2.1** XRF | Imaging of the brain
45… **1.3.2.2** XRF | Targeted imaging with nanoparticles

47… **THESIS STRUCTURE**

49… **2** **|CHEMISTRY |**
SYNTHESIS OF CARBOHYDRATE LEWIS^A,PHOTO-CROSSLINKER TRIFLUOROMETHYLPHENYLDIAZIRINE MOLECULES AND NANOPARTICLE FUNCTIONALISATION

51… **2.1** **| SYNTHESIS OF S-CYANOMETHYL-LEWIS^A**
51… **2.1.1** Rationale for using IME-based chemistry to couple Lewis^a onto amine nanoparticles
52… **2.1.2** Synthesis of monosaccharides of Lewis^a
54… **2.1.3** Glycosylation reactions to synthesise Lewis^a

56… **2.2** **| SYNTHESIS OF TRIFLUOROMETHYL-DIAZIRIN PHENYL-PROPANOIC ACID**
56… **2.2.1** Rationale for using trifluoromethyl-diazirin-phenyl-propanoic acid to couple onto amine-nanoparticles bearing Lewis^a
57… **2.2.2** Synthesis of the photo-crosslinker

59… **2.3** **| AMINE-NANOPARTICLE FUNCTIONALISATION**
59… **2.3.1** Determining the free amine content of commercial nanoparticles (MPIOs) and coupling conditions for photo-crosslinker
60… **2.3.2** Fmoc-numbering yields a quantitiative method to determinine amine-content on MPIOs and modification levels
61… **2.3.3** Dual functionalisation of nanoparticles with photo-crosslinker and Lewis^a
62… **2.3.4** Functionalisation of nanoparticles with the photo-crosslinker, Lewis^a and particle characteristics of treated particles
71… **2.3.5** Determining Lewis^a functionalisation levels of MPIO with an ELISA-based method

76… **2.4** **| DETERMINING THE PHOTO-CROSSLINKER REACTIVITY AND EFFECTIVENESS ON NANOPARTICLES**
76… **2.4.1** UV activation of trifluoromethyl-diazirin-phenyl-propanoic acid and the photo-crosslinker on MPIOs
76… **2.4.2** UV activation of trifluoromethyl-diazirin-phenyl-propanoic acid measured by FT-IR

78…	**2.4.3**	UV activation of photo-crosslinker modified MPIOs measured by FT-IR
78…	**2.4.4**	Photo-crosslinking of BSA to particles to determine crosslinking efficiency
82…	**2.4.5**	Optimising MPIO recovery from brain tissue
83…	**2.4.6**	Optimising MPIO recovery from brain tissue using bi-functional nanoparticles and photo-crosslinker nanoparticles
86…	**2.5**	**| DISCUSSION**
86…	**2.5.1**	Amine loading determination and the influence of solvent exposure on nanoparticle characteristics
88…	**2.5.2**	UV activation of the photo-crosslinker on MPIO *in vitro* is challenging
90…	**2.6**	**| CONCLUSION**
91…	**2.7**	**| METHODS**
91…	**2.7.1**	Reagents and buffers used
91…	**2.7.2**	Determination of (free) amine content on nanoparticles
92…	**2.7.3**	Coupling of photo-crosslinker onto SoluLink amine MPIO
93…	**2.7.4**	Free amine determination using Fmoc-numbering
94…	**2.7.5**	SCM-Le^{a} deprotection and IME-activation
94…	**2.7.6**	Bi-functional Lewis^{a}/diazirine photo-crosslinker MPIO
95…	**2.7.7.**	The effects of different aprotic solvents on the amine particles characteristics
97…	**2.7.8**	Rat E-Selectin *in vitro* screening experiment
98…	**2.7.9 .**	Le^{a} deprotection and IME-activation
99…	**2.7.10**	Coupling of IME-Le^{a} or Le^{b} onto amine MPIO
99…	**2.7.11.**	FT-IR monitoring of a diazo intermediate
100…	**2.7.12.**	FT-IR monitoring of a diazo intermediate on MPIO
101…	**2.7.13**	Buffers and reagents used for crosslinking experiments
101…	**2.7.14**	BSA crosslinking onto photo-crosslinker modified MPIO
102…	**2.7.15**	Buffers and reagents used for the recovery of MPIOs from the brain
103…	**2.7.16**	Recovery of MPIOs from an acute IL-1β brain inflammation model in rats
105…	**2.7.17**	Spike recovery of particles from brain tissue
106…	**2.7.18**	Magnet and dilution trial of spike recovery of particles from brain tissue
107…	**2.7.18.1**	Dynal magnet method
107…	**2.7.18.2**	Miltenyi magnet method
108…	**SI 2**	**|SUPPLEMENTARY INFORMATION CHAPTER 2|**
108…	**SI.2.1**	Synthesis of SCM-Lewis^{a}
115…	**SI.2.2**	Synthesis of Trifluoromethylphenyldiazirine
121…	**SI.3.3**	Additional IR spectra of UV-irradiated trifluoromethylphenyldiazirine
123…	**SI.3.4**	Additional IR spectra of UV-irradiated photo-crosslinker on MPIO

123… **3** **|BIOLOGY |**

***IN VITRO* AND *IN VIVO* CHARACTERIZATIONOF BRAIN INFLAMMATION MODELSUSING LEWIS^{A}-NANOPARTICLES**

125… **3.1** **| PROTEOME ANALYSIS OF LEWIS^{A} INTERACTING MOLECULES USING BI-FUNCTIONAL NANOPARTICLES *IN VITRO***

125… **3.1.1** Trapping multivalent carbohydrate interactions with nanoparticles using a photo-crosslinker and proteomics

126… **3.1.2** Design of the *in vitro* pull-down experiments using the bi-functional nanoparticles

129… **3.1.3** Calculations and anticipated results

131… **3.1.4** Pulldown experiments using the synthesised MPIOs

132… **3.1.5** Proteomic results using the bi-functional Lewis^{a}/photo-crosslinker pulldown particles yielded no lectins

132… **3.1.6** Proteomic results using the Lewis^{a} only pulldown particles also yields no lectins

135… **3.1.7** Proteome of bEnd.3 mouse brain microvascular endothelial cells stimulated with IL-1β reveals E-Selectin as the second highest upregulated protein

138… **3.2** **| TRANSCRIPTOMIC ANALYSIS OF ACUTE IL-1β BRAIN INFLAMMATION AND BCG MS-LIKE LESION MODEL**

142… **3.2.1** Transcriptome of IL-1β acute brain inflammation in adult and juvenile rats

148… **3.2.2** Transcriptome of MS-like lesions using a BCG inflammation model of chronic brain inflammation

150… **3.2.3** Comparing the transcriptome of chronic vs. acute brain inflammation

153… **3.3** **| *IN VIVO* LEWIS^{A} BLOCKING EXPERIMENTS OF ACUTE IL-1β BRAIN INFLAMMATION**

154… **3.3.1** *In vitro* binding of Lewis^{a}, Lewis^{b} and other Lewis antigens to E-Selectin and P-Selectin

157… **3.3.2** Considerations and overview of experimental details of the *ex vivo* MRI data presented

158… **3.3.3** Blood analysis of the experimental groups reveals an altered blood profile for IL-1β treated animals and shows effective neutrophil depletion for animals treated with an antiserum

163… **3.3.4** Lewis-MPIO quantification of the IL-1β inflamed brain using MRI

167… **3.3.4** Immunohistochemical analysis of E-Selectin and neutrophils in the experimental groups

170… **3.4** **| DISCUSSION**

170… **3.4.1** Proteomic pull down experiments and whole cell proteome

170… **3.4.1.1** Proteomics data comparison of pull down results yields no obvious lectins

171… **3.4.1.1** Selected other hits from Lewis^{a} only pull down

172… **3.4.2** Transcriptomic Experiments

172…	**3.4.2.1**	Overlapping transcriptomic results can be explained by neutrophils and platelets
174…	**3.4.2.2**	Brain derived neurotrophic factor (*Bdnf*)
174…	**3.4.2.3**	Collagen 1 alpha 1 (*Col1a1*)
175…	**3.4.2.4**	Transthyretin (*Ttr*)
178…	**3.4.2.5**	Lipocalin-2 (*Lcn2*), neutrophil gelatinase-associated lipocalin (NGAL)
179…	**3.4.2.6**	Oxytocin (*Oxt*)
179…	**3.4.2.7**	Other observations relating *Stra6* and *Col1a2*
180…	**3.4.3**	*In vivo* blocking experiments
180…	**3.4.3.1**	Proteomics, transcriptomics lead to Selectin-blockade and neutrophil depletion experiments
180…	**3.4.3.2**	Blood analysis and peripheral immunohistochemistry shows neutrophils are depleted *via* a liver-mediated mechanism
182…	**3.4.3.3**	Lewis^{a} binds strongly to E-Selectin *in vivo* and the interaction is blocked with monoclonal antibodies
184…	**3.4.3.4**	*In vitro* results can be misrepresentative and *in vivo* experiments confirms Lewis^{a} as the superior E-Selectin binder over sialyl-Lewis^{x}
185…	**3.4.3.5**	Lewis^{a} binds strongly to E-Selectin *in vivo* and the E-Selectin availability is dependent on the presence of neutrophils
188…	**3.5**	**|CONCLUSION**
189…	**3.6**	**| METHODS**
189…	**3.6.1**	Reagents and buffers used for the proteomics experiments
189…	**3.6.2**	Pulldown using bi-functional Lewis^{a}/Diazirine photo-crosslinker magnetic particles
191…	**3.6.3**	Pulldown using Lewis^{a} and amine magnetic particles
192…	**3.6.4**	Whole cell proteome of IL-1β treated mouse brain microvascular endothelial cells
193…	**3.6.5**	Proteomics data analysis details
194…	**3.6.6**	Acute IL-1β brain inflammation model in rats for transcriptomics
194…	**3.6.7**	Chronic BCG MS-Like brain inflammation model in rats for transcriptomics
195…	**3.6.8**	Data analysis of IL-1β brain inflammation model using R Script
195…	**3.6.9**	Data analysis of brain inflammation models using Affymetrix Expression Console (2014)
196…	**3.6.10**	Buffers and reagents used for the *ex vivo* MRI experiments
197…	**3.6.11**	Animals
197…	**3.6.12**	Rat E- and P-Selectin *in vitro* binding experiment
198…	**3.6.13**	Selectin blockade experiment
199…	**3.6.14**	Neutrophil depletion experiment
206…	**3.6.15**	Full blood count
206…	**3.6.16**	Immunohistochemistry for peripheral tissue
207…	**3.6.17**	Immunohistochemistry for brain tissue
209…	**3.6.18**	MRI imaging parameters for MPIO quantification

211… **SI 3** **|SUPPLEMENTARY INFORMATION CHAPTER 3|**
211… **SI.3.1** R Script
212… **SI.3.2** Additional time course graphs from the BCG MS-like lesion model in rats

220… **4** **| FUTURE APPLICATIONS |**
ELEMENTAL MAPPING OF BRAIN INFLAMMATION AND LEWIS^A-LABELLING OF EXTRACELLULAR VESICLES

222… **4.1** **| XRF IMAGING OF BRAIN INFLAMMATION USING XENOBIOTIC TARGETED NANOPARTICLES**
222… **4.1.1** Strategy for the generation of targeted XRF Imaging agents using the I18 beamline at Diamond
223… **4.1.2** Functionalisation of titanium oxide nanoparticle XRF probes with Lewis^a
223… **4.1.3** XRF Imaging of the generated XRF-Probes in brain sections at Diamond reveals Titanium contamination

228… **4.2** **| RETARGETING OF BIOLOGICAL NANOPARTICLES TO SITES OF BRAIN INFLAMMATION WITH LEWIS^A**
228… **4.2.1** Biological Functions of Lewis Antigens in Inflammation
229… **4.2.2** Labelling of extracellular vesicles for *in vivo* tracking
231… **4.2.3** miRNA and Lewis^a-lipid labelling of extracellular vesicles for *in vivo* brain inflammation targeting was unsuccessful
243… **4.2.4** Lewis^a-lipid labelling of fluorescent liposomes reveals *in vivo* brain inflammation targeting

235… **4.3** **|DISCUSSION**
235… **4.3.1** Lewis^a-mediated targeting of xenobiotic nanoparticles to brain inflammation sites was not observed by XRF imaging
236… **4.3.2** XRF analysis of acute IL-1β brain inflammation may reveal enzymatic activity
247… **4.3.3** Labelling of biological nanoparticles with a non-mammalian miRNA and a Lewis^a-lipid

239… **4.4** **|CONCLUSION**

240… **4.5** **| METHODS**
240… **4.5.1** Buffers and reagents used
240… **4.5.2** Le^a deprotection and IME-activation
241… **4.5.3** NP TiO_2-Le^a
241… **4.5.4** *In vivo* models of brain inflammation and XRF-probe administration
242… **4.5.5** Data analysis using the XRF-fitting software PyMca
244… **4.5.6** Immunohistochemical analysis of Lewis^a in mouse tissue

244… **4.5.7** Lewis^a-labelling and miRNA-transfection of EVs for acute brain inflammation targeting using qPCR
246… **4.5.8** Lewis^a detection in labelled extracellular vesicles for using a dot-blot
246… **4.5.9** Fluorescent tracking of Lewis^a-lipid labelled fluorescent liposomes *in vivo*

248… **5** **| SUMMARY AND FUTURE OUTLOOK |**

249… **5.1** **| SUMMARY**
249… **5.1.1** Principal findings of this thesis
251… **5.1.2** General Discussion
251… **5.1.2.1** The unknown role of Lewis^a in human during health and disease
251… **5.1.2.2** Lewis antigens and the vasculature
252… **5.1.2.3** Other Selectin imaging agents and the possible antigenicity of Lewis antigens
253… **5.1.2.4** Facile preparation of targeted liposomal delivery using Lewis antigens

254… **5.2** **| FUTURE OUTLOOK**

255… **REFERENCES**

| LISTING OF FIGURES AND TABLES |

9… **| Table 1.1 |** Cell adhesion molecules and their ligands

10… **| Figure 1.1 |** The multistep process of leukocyte recruitment and the receptor:ligand interactions involved

13… **| Figure 1.2 |** The cluster glycoside effect allows multivalent interactions between PSGL-1 on neutrophils and E-Selectin on endothelial cells

14… **| Figure 1.3 |** Overview of Type 1 (Lewis^{a} and Lewis^{b}) and Type 2 (Lewis^{x} and Lewis^{y}) structures used on MPIO in the pilot experiment presented in Figure 1.4.

15… **| Figure 1.4 |** Pilot experiment to assess the binding of Lewis antigens Lewis^{a}, Lewis^{b}, Lewis^{x} and Lewis^{y} during a model of acute brain inflammation in rodents

17… **| Table 1.2 |** Overview of fucosyl transferases and the Lewis antigens

18… **| Figure 1.5 |** Overview of the the fucosyltransferases, linkages and types of carbohydrate present in the Lewis antigens

21… **| Table 1.3 |** Binding of mammalian transfected cells expressing human E-Selectin to Lewis antigens as neoglycolipids run on thin-layer chromatographic plates

21… **| Table 1.4 |** Binding of recombinant human E-Selectin to Lewis antigens as neoglycolipids run on thin-layer chromatographic plates

21… **| Table 1.5 |** Binding of recombinant E- and P-Selectin to Lewis antigens immobilized onto bovine serum albumin

21… **| Table 1.6 |** Binding of human colon cancer cell lines to biotinylated Lewis antigens

24… **| Figure 1.6 |** Pilot experiment to assess the binding of Le^{a}-MPIO in SIGN-R3 knock-out mice during a model of acute brain inflammation

29… **| Figure 1.7 |** Extracellular vesicles: cellular origin, size range and uptake mechanism

31… **| Table 1.7 |** MRI signals of CNS tissue using different magnetisation sequences

32… **| Figure 1.8 |** T_1, T_2 and T_2^* MRI signals and the interaction of protons with induced magnetic fields

35… **| Figure 1.9 |** Binding of Le^{a}-MPIO in a MS-lesion like model in the rat brain

39… **| Figure 1.10 |** Photo-crosslinker structures and mechanisms of protein cross linking

44… **| Figure 1.11 |** XRF principals

44… **| Figure 1.12 |** XRF emission lines compatible with the I18-Beamline at Diamond, Didcot UK

51… **| Figure 2.1 |** IME-Lewis^{a} enables amine-nanoparticle modification using mild aqueous conditions

53… **| Figure 2.2 |** Synthesis scheme for the reactions yielding the monosaccharides for SCM-Lewis^{a}

55… **| Figure 2.3 |** Synthesis scheme of the glycosylation reactions for SCM-Lewis^{a}: the precursor of IME-Lewis^{a}

58… **| Figure 2.4 |** Synthesis scheme for the synthesis of trifluoromethyl-diazirin-phenyl-propanoic acid used to generate the bi-functional pull down particles

59… **| Figure 2.5 |** Chemistry of the commercial MPIO used

60… **| Table 2.1 |** Amine-reactive detection methods explored in this thesis

60… **| Table 2.2 |** Different coupling conditions for Fmoc-numbering

62… **| Table 2.3 |** Overview of the batches reported in thesis and experiments conducted

62… **| Table 2.4 |** Coverage calculations (305 nm) of MPIO-NH_2 using different equivalants of a photo-crosslinker mimic

63… **| Figure 2.6 |** Coverage control of the amount of functionlised amines on amine-nanoparticles (MPIO) using 3-(4-bromophenyl) propanoic acid

64… **| Figure 2.7 |** Amine functionalisation coverage of pulldown particles (MPIO) using the photo-crosslinker and Lewis^{a}

65… **| Table 2.5 |** Coverage control of MPIO-NH_2 using substoichiometric amounts of coupling agent and the diazirine photo-crosslinker

65… **| Figure 2.8 |** Coverage determination of MPIO-NH_2 functionalised with the photo-crosslinker as measured by Fmoc-numbering

66… | **Figure 2.9 |** Coverage determination of MPIO-NH_2 functionalised with the photo-crosslinker and Lewis[a] as measured by Fmoc-numbering

66… **|Table 2.6 |** Size (nm), charge (ζ) and coverage (Fmoc) of MPIO-NH_2 covered with a photo-crosslinker and Lewis[a]

68… | **Figure 2.10 |** Overview of amine-coverage (Fmoc), charge (ζ) and size (nm) of MPIO-NH^2 particle characteristics presented in Table 2.6

69… | **Figure 2.11 |** Overview of size (nm) and charge (ζ, mV) of the different solvent-treated MPIO particles using a Malvern Zetasizer Nano ZS

70… | **Figure 2.12 |** Size measurement comparison of the two different DLS machines

71… | **Figure 2.13 |** Schematic of the assay principle using the Perls' Prussian Blue stain

72… | **Figure 2.14 |** The influence of washing on the E-Selectin : Lewis[a]-MPIO interaction and binding measured by the Perls' Prussian Blue ELISA method

73… | **Figure 2.15 |** The influence of Calcium-chelation on the E-Selectin : Lewis[a]-MPIO interaction and binding measured by the Perls' Prussian Blue ELISA method

74… | **Figure 2.16 |** Rapid screening method for Lewis[a] and Lewis[b] functionalised MPIO batches using the Perls' Prussian Blue ELISA method

75… **|Table 2.7 |** Coverage of MPIO-NH2 and Lewis[a] and Lewis[b] functionalised MPIO measured by Fmoc-numbering

75… | **Figure 2.17 |** Graph of the measured coverage of MPIO-NH_2 and Lewis[a] and Lewis[b] functionalised MPIO using Fmoc-numbering

77… | **Figure 2.18 |** The formation of a diazo intermediate upon UV exposure of the photo-crosslinker

79… **| Table 2.8 |**Photo-crosslinked BSA peptides can be cleaved from PXL-MPIO with trypsin

79… **| Table 2.9 |**Efficiency of photo-crosslinking and the amount of PXL molecules present per BSA molecule

79… | **Figure 2.19 |** Comparison of trypsin cleaved, isolated BSA peptides from PXL- and NH_2-MPIO incubated with BSA and UV light

80… | **Figure 2.20 |** Comparison of isolated BSA peptides from UV-treated and non UV-treated PXL- and NH_2-particles incubated with BSA

80… | **Table 2.10 |** Trypsin-cleaved BSA peptides from PXL-MPIO and NH_2-MPIO treated with UV light and a non UV-treated control

81… **| Figure 2.21 |**Size considerations of the nanoparticles, BSA and the photo-crosslinker

83… | **Figure 2.22 |** Recovery of particles from the left IL-1β inflamed striatum from animals injected with bi-functional MPIOs and photo-crosslinked modified MPIOs

83… | **Table 2.11 |** Recovery of the particles from the left IL-1β inflamed striatum from animals injected with bi-functional MPIOs and photo-crosslinked modified MPIOs

84… | **Figure 2.23 |** Spike recovery of particles from H_2O, RIPA buffer and brain homogenate to assess isolation yield

85… | **Figure 2.24 |** Spike recovery of particles comparing different magnets and brain homogenate dilutions

88… | **Figure 2.25 |** Model for the increased numbers of amines after solvent exposure

95… | **Figure 2.26 |** Overview of particle treatment to test the effects of aprotic solvent exposure

102… **| Table 2.12 |**Protein concentration of the wash supernatant

102… | **Figure 2.27 |** NanoDrop trace of photo-crosslinked BSA peptides cleaved off PXL-MPIO particles with trypsin

104… | **Figure 2.28 |** Dissection guide to obtain left striatum

105… | **Table 2.13 |** Overview of experiment

129… | **Figure 3.1 |** Experimental overview and design of a bi-functional Lewis[a]/Diazirine photo-crosslinker magnetic pull down tool for proteomics *in vitro*

130… | **Figure 3.2 |** Cell size considerations of a model of an endothelial cell binding Lewis[a] MPIO

131… | **Table 3.1 |** Data nomenclature and experimental overview for proteomics files using pulldown particles

133… **| Table 3.2 |** Data summary of bi-functional Lewis[a]/Diazirine photo-crosslinker magnetic particle pulldown on GP8.3 rat brain microvascular endothelial cells

134… **| Table 3.3 |** Data summary of Lewis[a] magnetic particle pulldown on GP8.3 rat brain microvascular endothelial cells

136… **| Table 3.4 |** Data summary of whole cell proteome of bEnd.3 mouse brain microvascular endothelial cells stimulated with IL-1β reveals E-Selectin as the second highest and VCAM-1 as the highest upregulated proteins

139… **| Figure 3.3 |** Experimental overview of GeneChip® experiment using IL-1β as a model of brain inflammation

140… **| Table 3.5 |** *N*-numbers of experiments and GeneChip-runs

140… **| Figure 3.4 |** Experimental overview of GeneChip® experiment using BCG as a model of MS-like brain inflammation

141… **| Figure 3.5 |** Results of mRNA transcripts upregulated by IL-1β during brain inflammation in the adult and juvenile rat

144… **| Table 3.6 |** Overview of selected immune-related transcripts and their functions

145… **| Table 3.7 |** Data summary of IL-1β upregulated mRNA transcripts in adult rat brains reveals E-selectin as the third highest upregulated gene

146… **| Table 3.8 |** Data summary of IL-1β upregulated mRNA transcripts in juvenile rat brains reveals E-selectin as the third highest upregulated gene

147… **| Table 3.9 |** Data summary of BCG lesion specific upregulated mRNA transcripts compared to vehicle treated and naïve brains

151… **| Figure 3.6 |** Gene expression profiles over time comparing BCG lesions to vehicle and naïve lesions

152… **| Figure 3.7 |** Gene expression profiles comparing adult and juvenile IL-1β lesions to vehicle

154… **| Figure 3.8 |** Experimental overview *in vivo* Lewis[a] and Lewis[b] blocking experiments of acute IL-1β brain inflammation

155… **| Figure 3.9 |** Binding of Lewis[a/b]-MPIO to rat recombinant E- and P-Selectin reveals no significant difference in binding between the Lewis antigens and the Selectins

156… **| Figure 3.10 |** Binding of Lewis antigens on MPIO to rat recombinant E- and P-Selectin shows that Lewis[a] binds E-Selectin at lower concentrations

156… **| Table 3.10 |** Lewis-antigens used for the E- and P-Selectin ELISA

157… **| Figure 3.11 |** Variable experimental timings resulted in altered Lewis[a/b]-MPIO binding

157… **| Figure 3.12 |** Overview of coronal MRI sections of a rat brain used to generate Z-stacks

158… **| Figure 3.13 |** Representative ROIs for image analysis

159… **| Table 3.11 |** Tabular overview of full blood counts of the experiments used for statistical analysis

159… **| Table 3.12 |** Overview of data comparison groups for statistics

160… **| Figure 3.14 |** Absolute Cell numbers of the experimental groups shows an altered white blood cell composition and effective neutrophil depletion in the antiserum treated animals

161… **| Figure 3.15 |** Blood parameters of the experimental groups studied for Lewis[a/b]-MPIO binding – Graphs 1

162… **| Figure 3.16 |** Blood parameters of the experimental groups studied for Lewis[a/b]-MPIO binding – Graphs 2

164… **| Figure 3.17 |** Quantified MRI analysis of the hemisphere and basal ganglia (BG) reveals E-Selectin mediated Lewis[a]-MPIO binding and E- and P-Selectin medated binding for Lewis[a]-MPIO during the Selectin Blockade experiments

165… **| Figure 3.18 |** Quantified MRI analysis of hemisphere and basal ganglia shows a role for neutrophils in the binding of Lewis[a/b]-MPIO during the neutrophil depletion experiments

166… **| Figure 3.19 |** Representative Z-stacks of MRI images of the Selectin Blockade and Neutrophil Depletion experiments performed

168… **| Figure 3.20 |** Immunohistochemical analysis of E-Selectin Expression in brains of Lewis[a]-MPIO animals reveals E-Selectin expression in all treatment groups

169… **| Figure 3.21 |** Immunohistochemical quantification of neutrophils in peripheral tissue of Lewis^a-MPIO animals

169… **| Figure 3.22 |** Neutrophil blood numbers for the Selectin Blockade Experiment shows a difference between Lewis^a and Lewis^b

173… **| Figure 3.23 |** The role of Collagen and BDNF in brain inflammation

176… **| Figure 3.24 |** The role Transthyretin in brain inflammation

177… **| Figure 3.25 |** The role of Oxytocin and Lcn-2 in brain inflammation

181… **| Figure 3.26 |** Liver-mediated neutrophil clearance

183… **| Figure 3.27 |** Lewis^a-MPIO binding is dependent on the availably of E-selectin

185… **| Figure 3.28 |** Proposed *in vivo* model to explain the observed strong Lewis^a binding compared to its β3-linkage isoform Lewis^b and sialyl-Lewis^x and the interaction with neutrophils, platelets and the inflamed endothelium *via* the Selectins

200… **| Figure 3.29 |** MRI Z-Stacks for Lewis^a-MPIO binding – Overview 1 E- and P-Selectin Block

201… **| Figure 3.30 |** MRI Z-Stacks for Lewis^a-MPIO binding – Overview 2 Isotype Controls

202… **| Figure 3.31 |** MRI Z-Stacks for Lewis^a-MPIO binding – Neutrophil Depletion

203… **| Figure 3.32 |** MRI Z-Stacks for Lewis^b-MPIO binding – Overview 1 E- and P-Selectin Block

204… **| Figure 3.33 |** MRI Z-Stacks for Lewis^b-MPIO binding – Overview 2 Isotype Controls

205… **| Figure 3.34 |** MRI Z-Stacks for Lewis^b-MPIO binding – Neutrophil Depletion

209… **| Table 3.13 |** Antibodies used for immunohistochemistry

212… **| Supplemental Table 3.1|** Data summary of gene expression transcripts over time comparing BCG lesions to vehicle lesions

216… **| Supplemental Table 3.2|** Data summary of gene expression transcripts over time comparing

223… **| Figure 4.1 |** Ti-nanoparticle functionalisation with IME-Lewis^a

224… **| Figure 4.2 |** XRF elemental map of brain inflammation using the NP TiO_2-Lewis^a XRF probe reveals a Ti-contamination in the untreated brain

225… **| Figure 4.3 |** XRF Ti-hotspot analysis reveals the Ti-contamination

226… **| Figure 4.4|** An XRF elemental map of endogenous elements in the inflamed brain

227… **| Figure 4.5 |** An XRF elemental map of Cu (copper) in the inflamed brain shows Cu-hotspots on the left IL-1β inflamed side

230… **| Figure 4.6 |** Experimental overview of targeting labelled EVs with a Lewis^a-lipid and a non-mammalian miRNA using the IL-1β brain inflammation model

231… **| Figure 4.7 |** Lewis^a-lipid labelling of endothelial cell derived EVs and detection of labelling using denaturing and native dot-blots

232… **| Figure 4.8 |**qPCR cycle threshold (CT) values of the spike-ins and the cel-mIR-39-3p in selected tissues

233… **| Figure 4.9 |** Lewis^a-lipid labelling of fluorescent liposomes

234… **| Figure 4.10 |** Fluorescence microscopy images of organ sections taken from mice injected with fluorescent liposomes labelled with Lewis^a-lipid to target the IL-1β inflamed brain

237… **| Figure 4.11 |**Steric hindrance model of Lewis^a presented on extracellular vesicles

242… **| Table 4.2 |** Experimental overview

243… **| Figure 4.21|** XRF fitting parameters using PyMca software (version 4.7.4)

244… **| Figure 4.22 |** Immunohistochemical analysis of Lewis^a structures in mice